Supporting Information

## Structural Basis for Cu(II) Metallocycle Hexamer Formation

Matthew L. Bracken,[*a] Manuel A. Fernandes, [a] Daniel Wamwangi[b,c] and Orde Q. Munro[a,d]

[a]University of the Witwatersrand, Molecular Sciences Institute, South Africa

[b]School of Physics, University of the Witwatersrand, Wits 2050, Johannesburg, South Africa

[c]DSI-NRF Centre of Excellence in Strong Materials, University of the Witwatersrand, Wits 2050, Johannesburg, South Africa

[d]University of Leeds, Department of Chemistry, UK

## S1 ORTEP Diagrams



**S1.1**: Thermal ellipsoid diagram of the asymmetric unit of **Cu1** where all atoms are shown at 50% probability level.
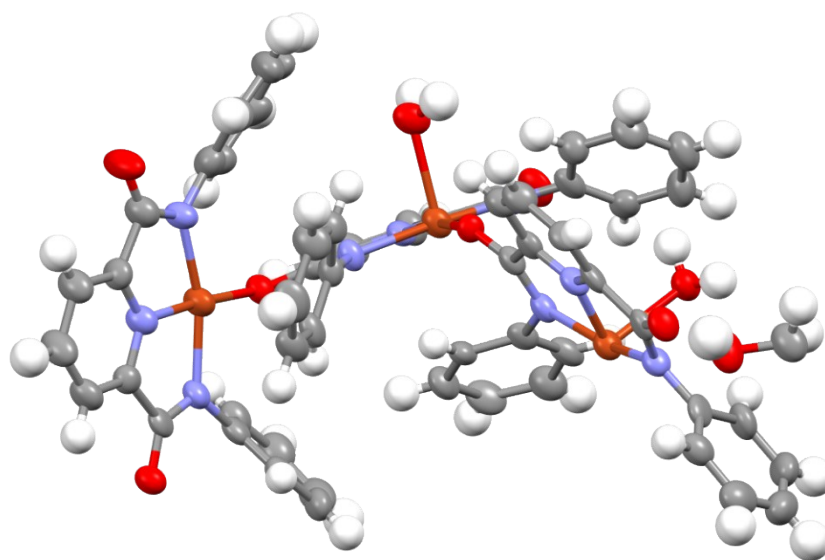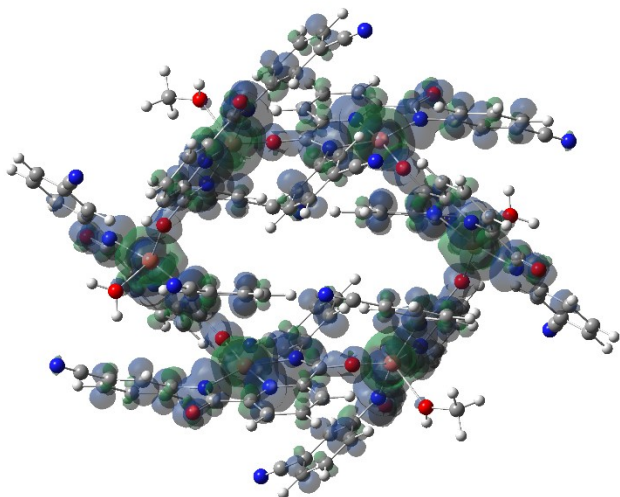
**S1.2**: Thermal ellipsoid diagram of the asymmetric unit of **Cu2** where all atoms are shown at 50% probability level.



**S1.3**: Thermal ellipsoid diagram of the asymmetric unit of **Cu3** where all atoms are shown at 50% probability level.

# S2 Computational



**S2.1**: **Cu1** calculated at the b3lyp/lan2dz level of theory. The spin density plot shonws significant $3d_{x^2-y^2}$ character and electron density is dispersed over the cyclic assembly. Hence, antiferromagnetic coupling is likely affecting the stability of the metallocycle, where spin coupling has lowered the potential energy of the superstructure.
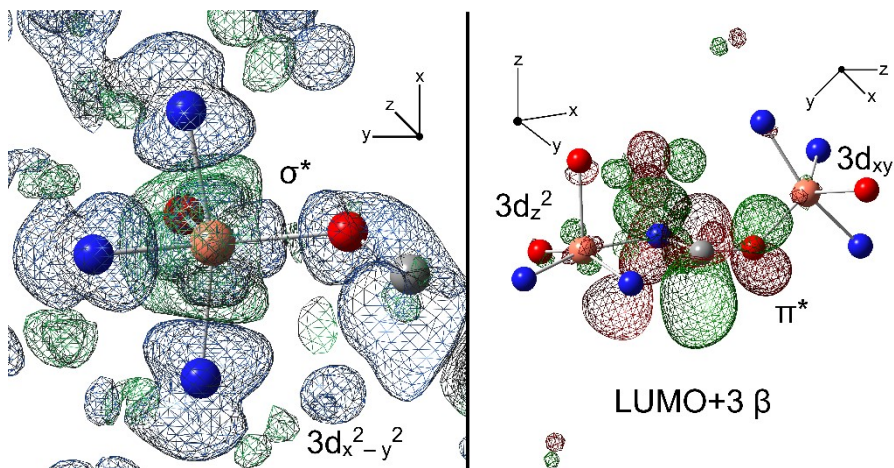


**S2.2**: The inner coordinations sphere of **Cu1** calculated at the b3lyp/lan2dz level of theory showing the spin-density on the left, and the LUMO +3 on the right. The spin-density plot shows the bridging carbonyl interaction is dominated by σ-overlap between the metal-based $3d_{x^2-y^2}$ orbital and σ* MO of the carbonyl. The LUMO shows additional antibonding involving π-overlap of the copper-based $3d_{xy}$ orbital and the π* MO of the bridging carbonyl. Additionally, the axially coordinated solvent molecule shows significant $3d_{z^2}$ character, substantiating the claim that the z-axis is collinear with the axial position.
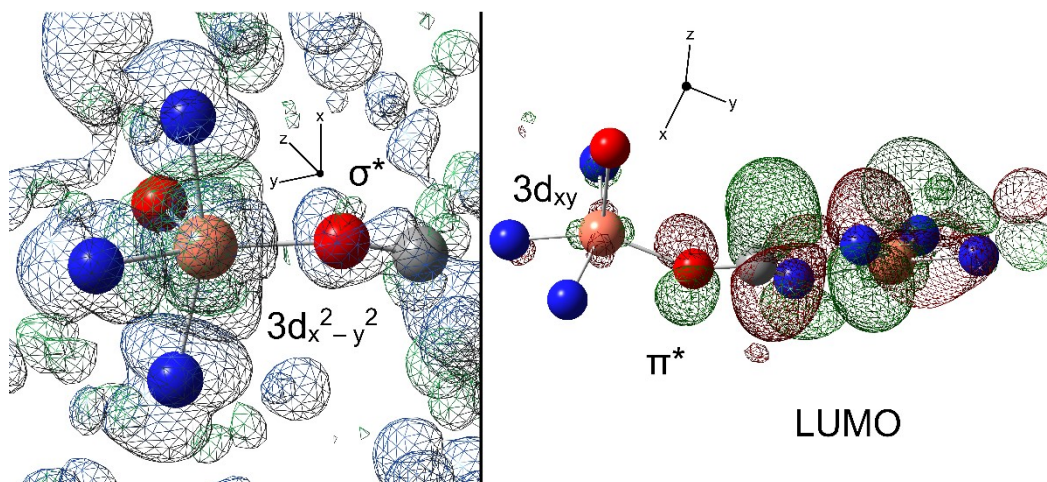
**S2.3**: The inner coordinations sphere of **Cu2** calculated at the b3lyp/lan2dz level of theory showing the spin-density on the left, and the LUMO on the right. The spin-density plot shows the bridging carbonyl interaction is dominated by σ-overlap between the metal-based $3d_x{}^2{}_{-y}{}^2$ orbital and σ* MO of the carbonyl. The LUMO shows additional antibonding involving π-overlap of the copper-based $3d_{xy}$ orbital and the π* MO of the bridging carbonyl.
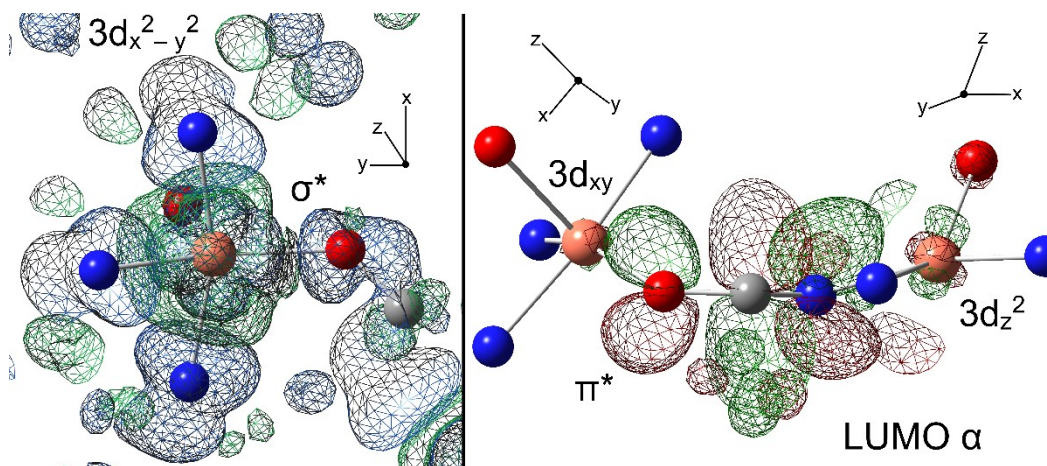


**S2.4**: The inner coordinations sphere of **Cu3** calculated at the b3lyp/lan2dz level of theory showing the spin-density on the left, and the LUMO +3 on the right. The spin-density plot shows the bridging carbonyl interaction is dominated by σ-overlap between the metal-based $3d_x{}^2{}_{-y}{}^2$ orbital and σ* MO of the carbonyl. The LUMO shows additional antibonding involving π-overlap of the copper-based $3d_{xy}$ orbital and the π* MO of the bridging carbonyl. Additionally, the axially coordinated solvent molecule shows significant $3d_z{}^2$ character, substantiating the claim that the z-axis is collinear with the axial position.
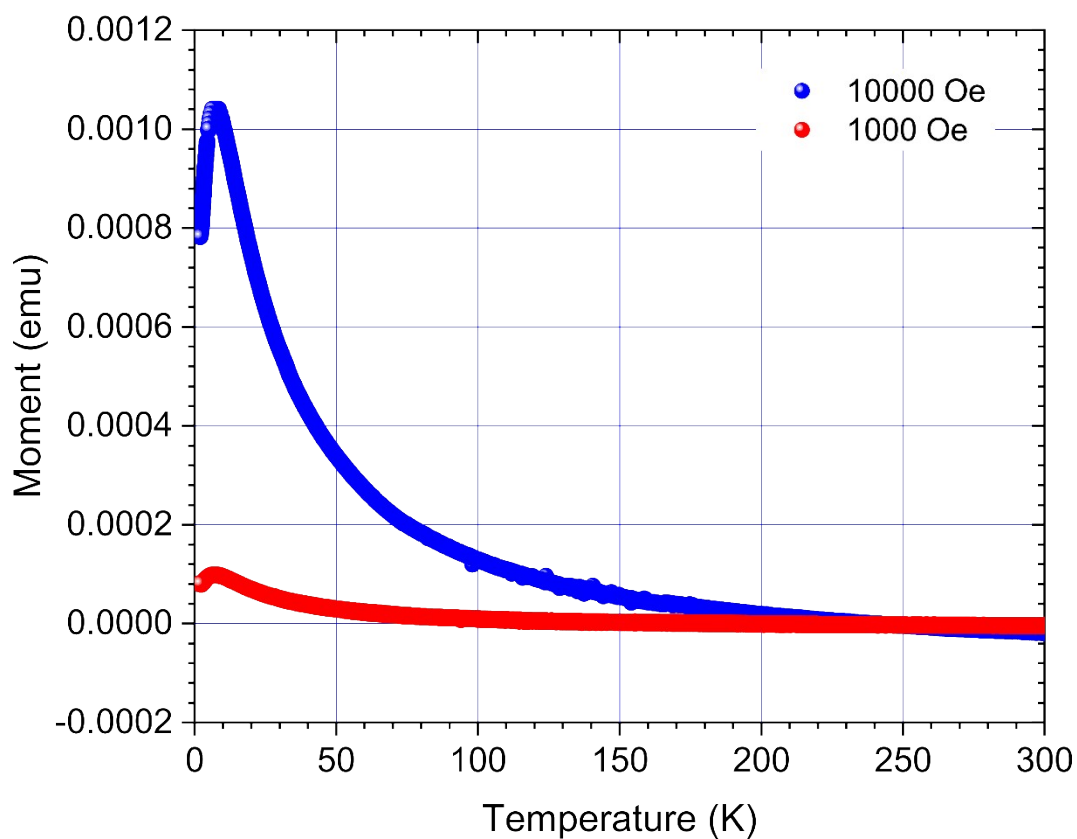
S3 Magnetic Measurements
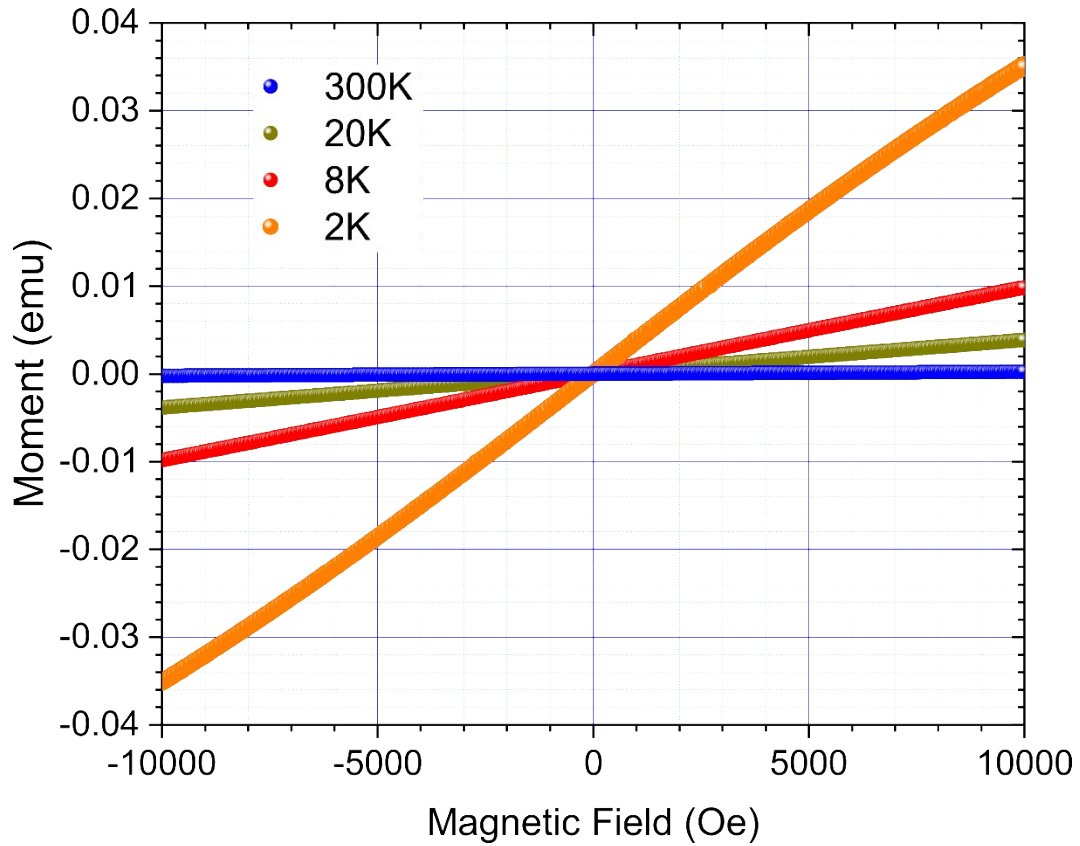


Isotherm Curves of **Cu1**
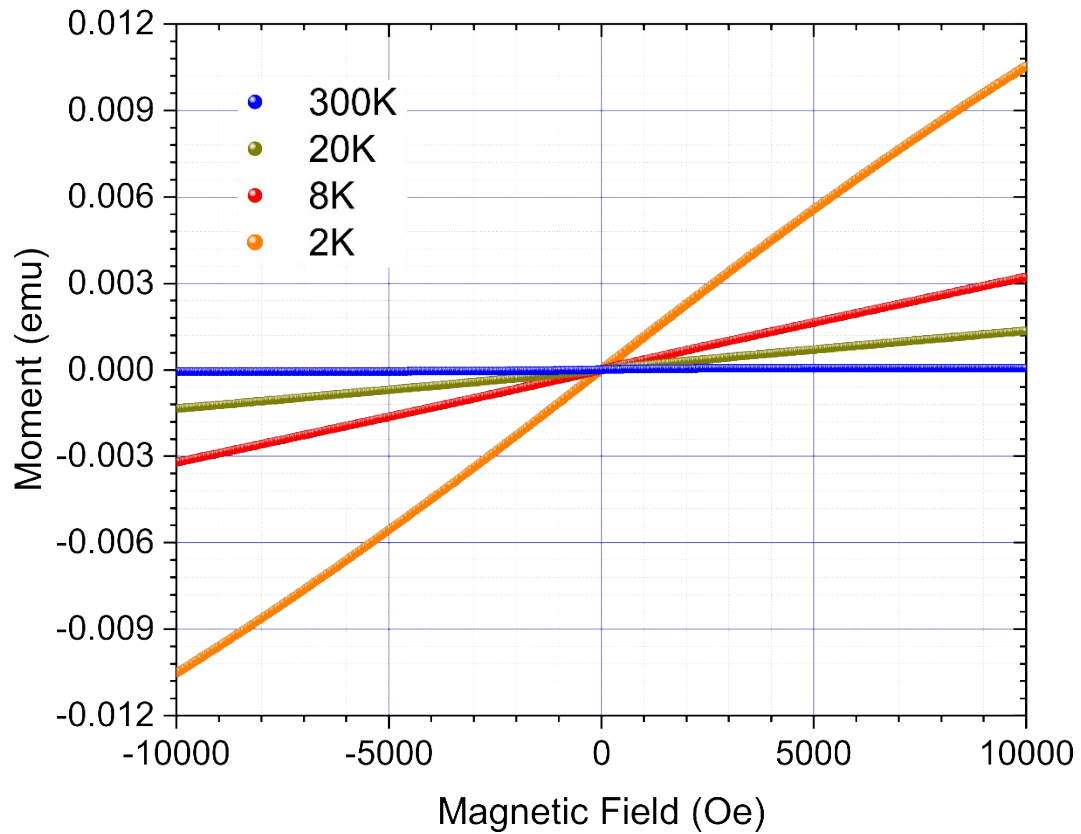
**S3.1**: Isotherm curves for **Cu1** between 300 and 2 K. There is soft ferromagnetism at 300 K which transforms to ferromagnetism with paramagnetism at 100 K. At 2 K there is an antiferromagnetic structure inducing a paramagnetic effect. These data indicate magnetic ordering.
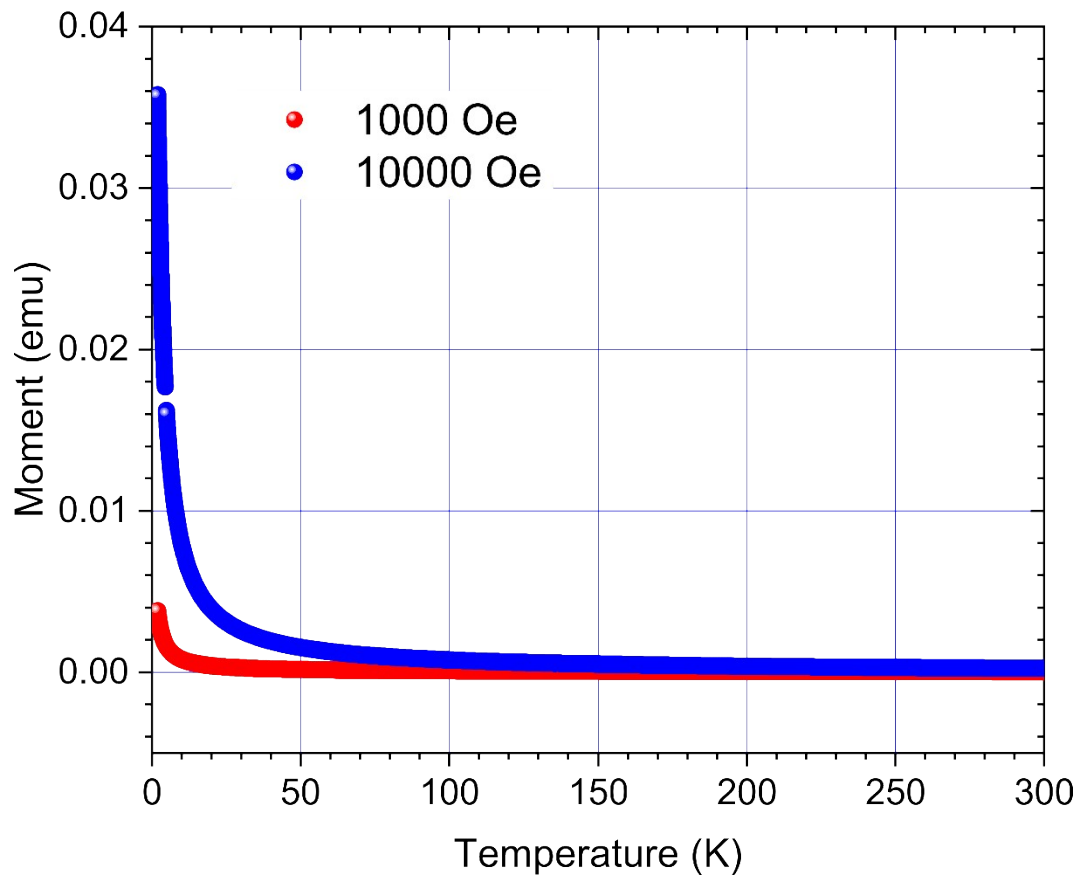
# Isofield Curves for **Cu1**



**S3.2**: Isofield curves for **Cu1** at 1000 and 10000 Oe. There are low temperature antiferromagnetic signatures at T < 8.3 and 9.3K, for 1 and 0.1T, respectively. It is seen that the Neel temperature is field dependent. Antiferromagnetic exchange interactions transferred through C-N-O$_{amide}$ supported by DFT spin-density plots.

## Isotherm Curves of **Cu2**

Legend:
- 300K
- 20K
- 8K
- 2K

Y-axis: Moment (emu), from -0.04 to 0.04
X-axis: Magnetic Field (Oe), from -10000 to 10000

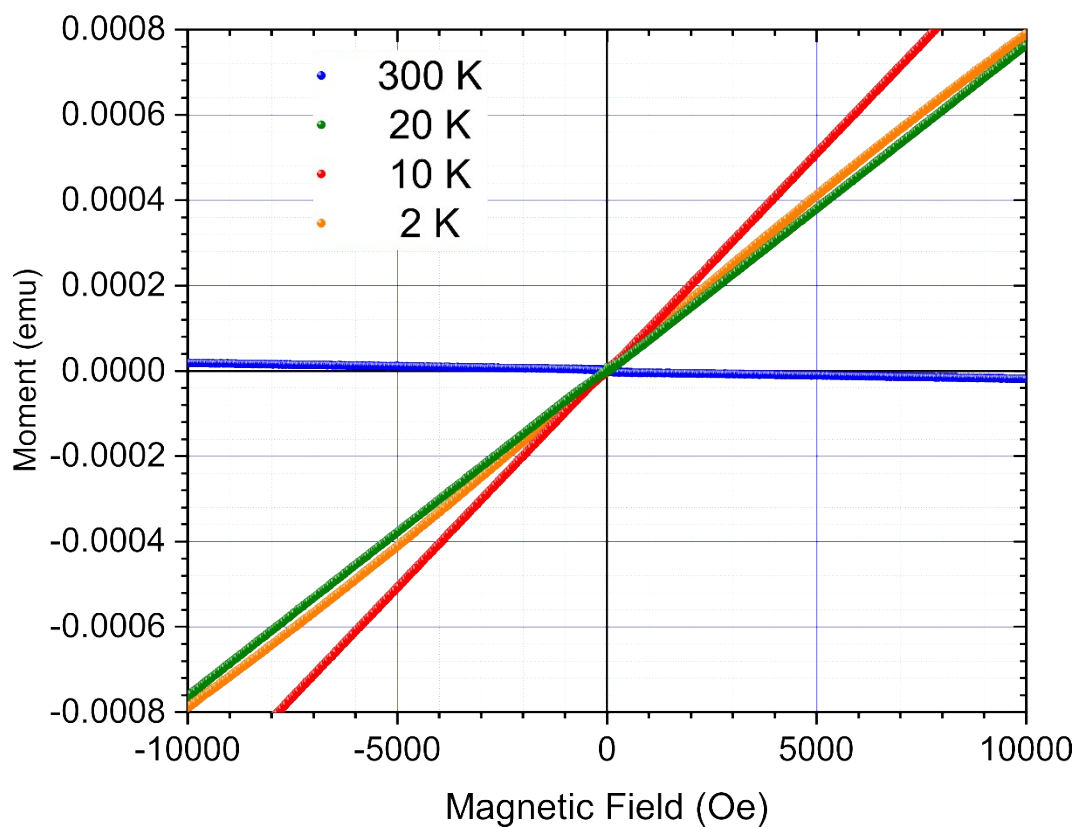**S3.3**: Isotherm curves for **Cu2** between 300 and 2 K. Below the Neel temperature T < 8 K, we have antiferromagnetic and super-paramagnetic phases. At T > 8 K, a paramagnetic structure emerges which decreases with increasing temperature. The super-paramagnetic phase at low temperature indicates magnetic ordering.
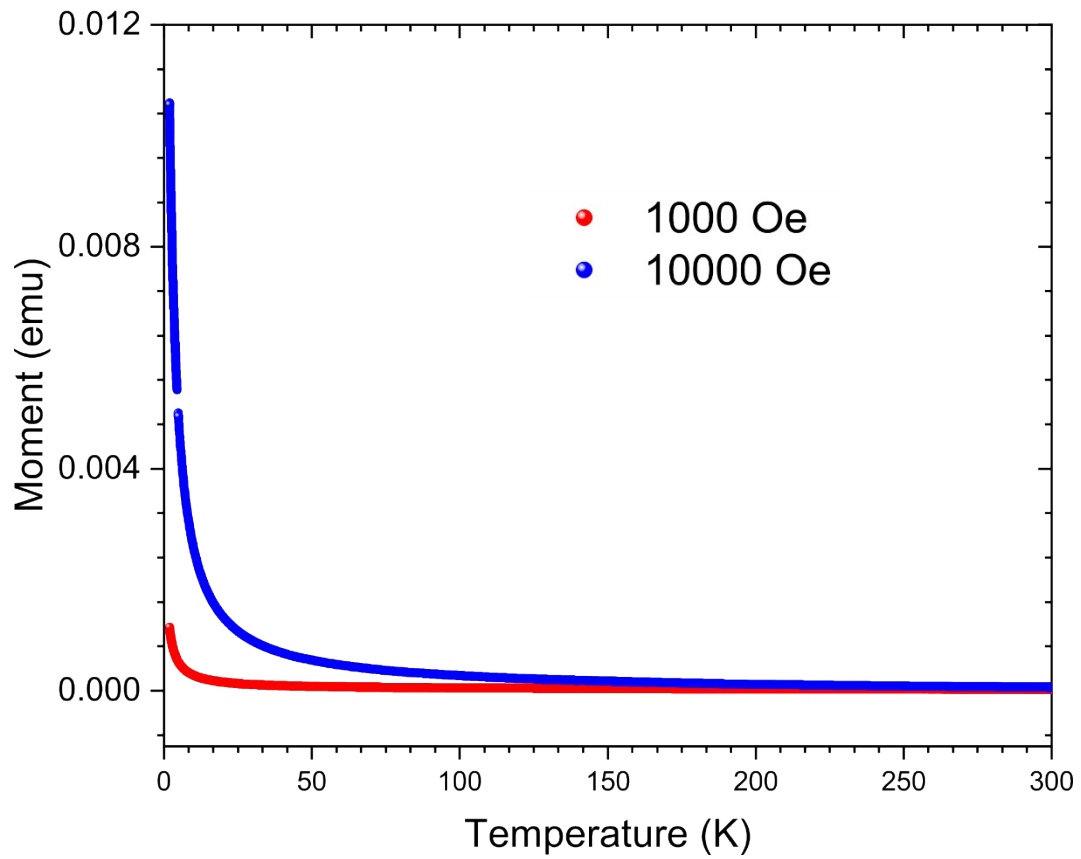
**S3.4**: Isofield curves for **Cu2** at 1000 and 10000 Oe. Below the Neel temperature T < 8 K, we have antiferromagnetic and super-paramagnetic phases.

Isotherm Curves of **Cu3**

**S3.5**: Isotherm curves for **Cu3** between 300 and 2 K. The solid sample is diamagnetic at 300 K indicating unpaired electrons in the metallocycle respond to an applied field to become ordered at room temperature. At 100 K, there is a moment reversal as **Cu3** becomes paramagnetic. There is complete paramagnetism at 2 K.

**S3.6**: Isofield curves for **Cu3** at 1000 and 10000 Oe. The sample shows no exchange interactions at low temperature.

# S4 Tensegrity
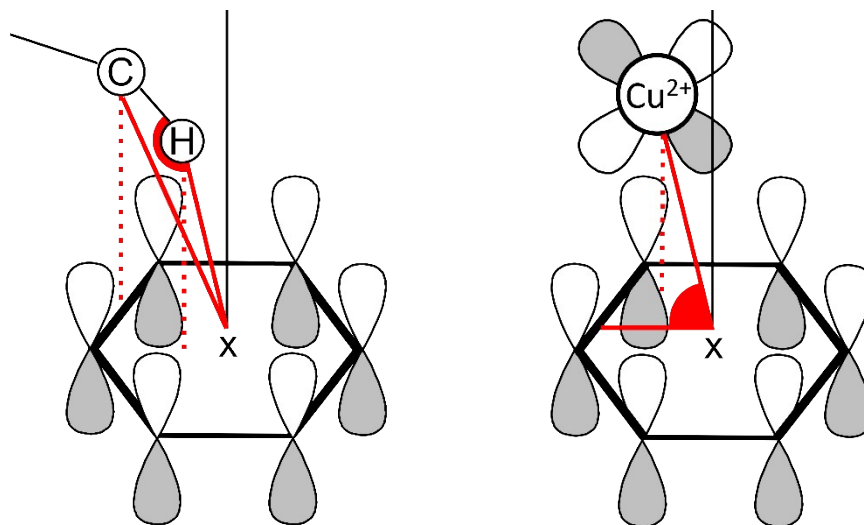


**S4.1**: The geometry of C–H···π and d···π interactions. The centroid of the aromatic ring is marked "x" and the normal to the aromatic plane is shown as a solid black line. The atom-to-centroid distances are marked by solid red lines while atom-to-plane distances are marked by dashed red lines. The angles that define the interaction have been marked in red. The C–H···π interaction has optimal overlap when the angle at hydrogen ∠C–H–X approaches 180°. The metal d···π interaction has optimal overlap when the angle at the centroid ∠C–X–M approaches 90°. The angle is defined by selecting the atom in the aromatic ring closest to the metal centre, the centroid of the ring, and the metal centre itself. When the d···π interaction has optimal overlap all angles ∠C–X–M will approach 90° as the $dz^2$ orbital approaches the centroid of the aromatic ring. When the d···π interaction angle ∠C–X–M is acute, but greater than 45°, the $d_{xz}$ and $d_{yz}$ orbitals are orientated for favourable overlap with the π molecular orbitals of the aromatic ring. Hence, C–H···π interactions will be described by the atom-to-plane distance between the hydrogen atom and the aromatic plane as well as the angle at hydrogen ∠C–H–X. Furthermore, d···π interactions will be described by the atom-to-plane distance in angstroms between the metal centre and the aromatic plane as well as the angle at the centroid ∠C–X–M.
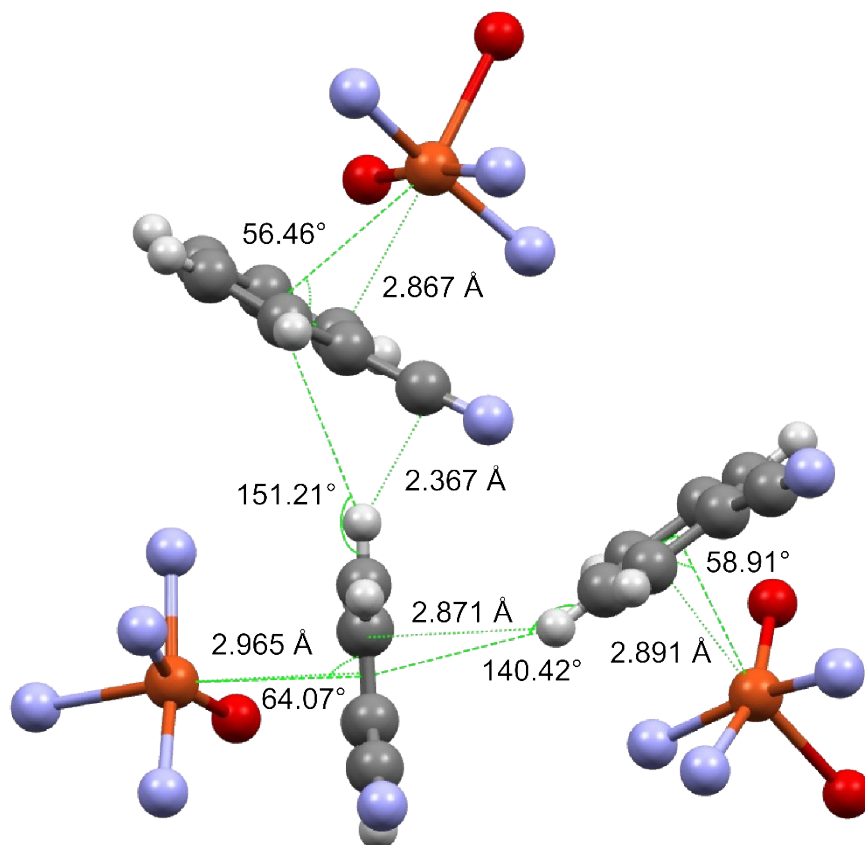
**S4.2**: C–H···π and d···π interactions for **Cu1**. Due to nitrile group in 3-position the third C–H···π interaction is unable to form.

**S4.3**: C–d···π for **Cu2**.
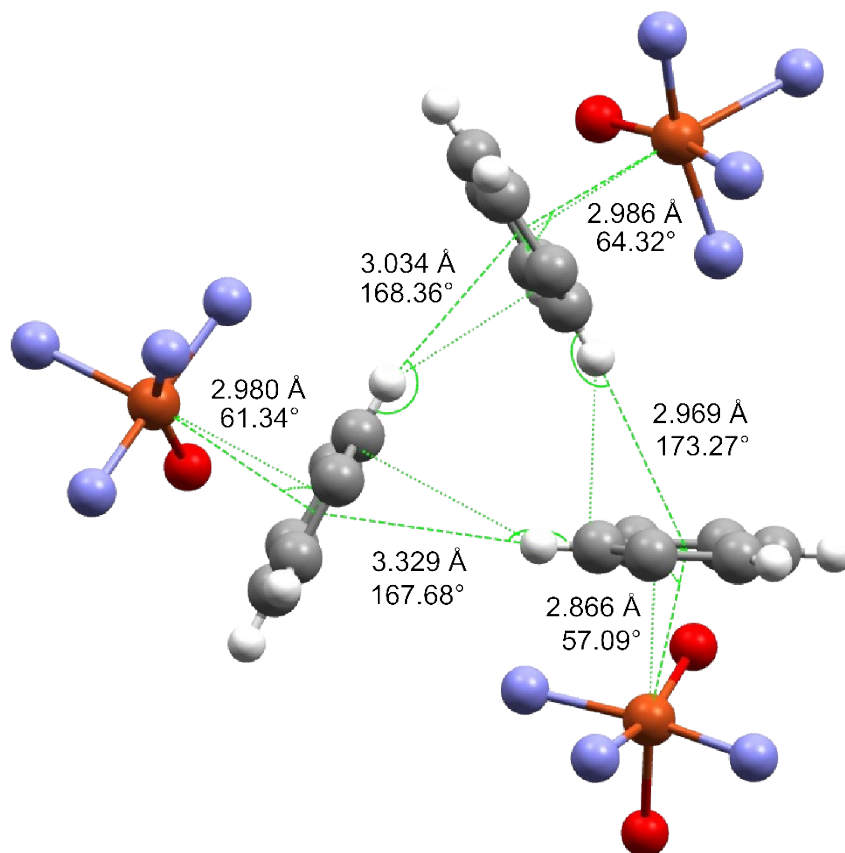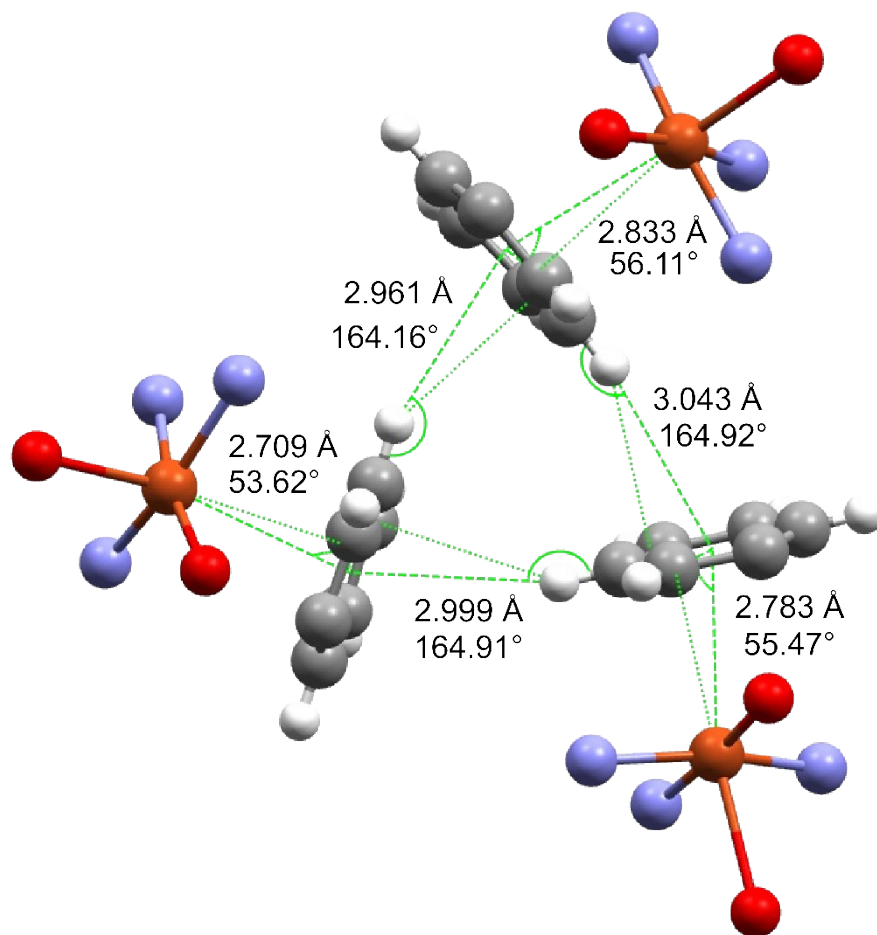
H···π and interactions

**S4.4**: C–H⋯π and d⋯π interactions for **Cu3**.

# S5 Voids
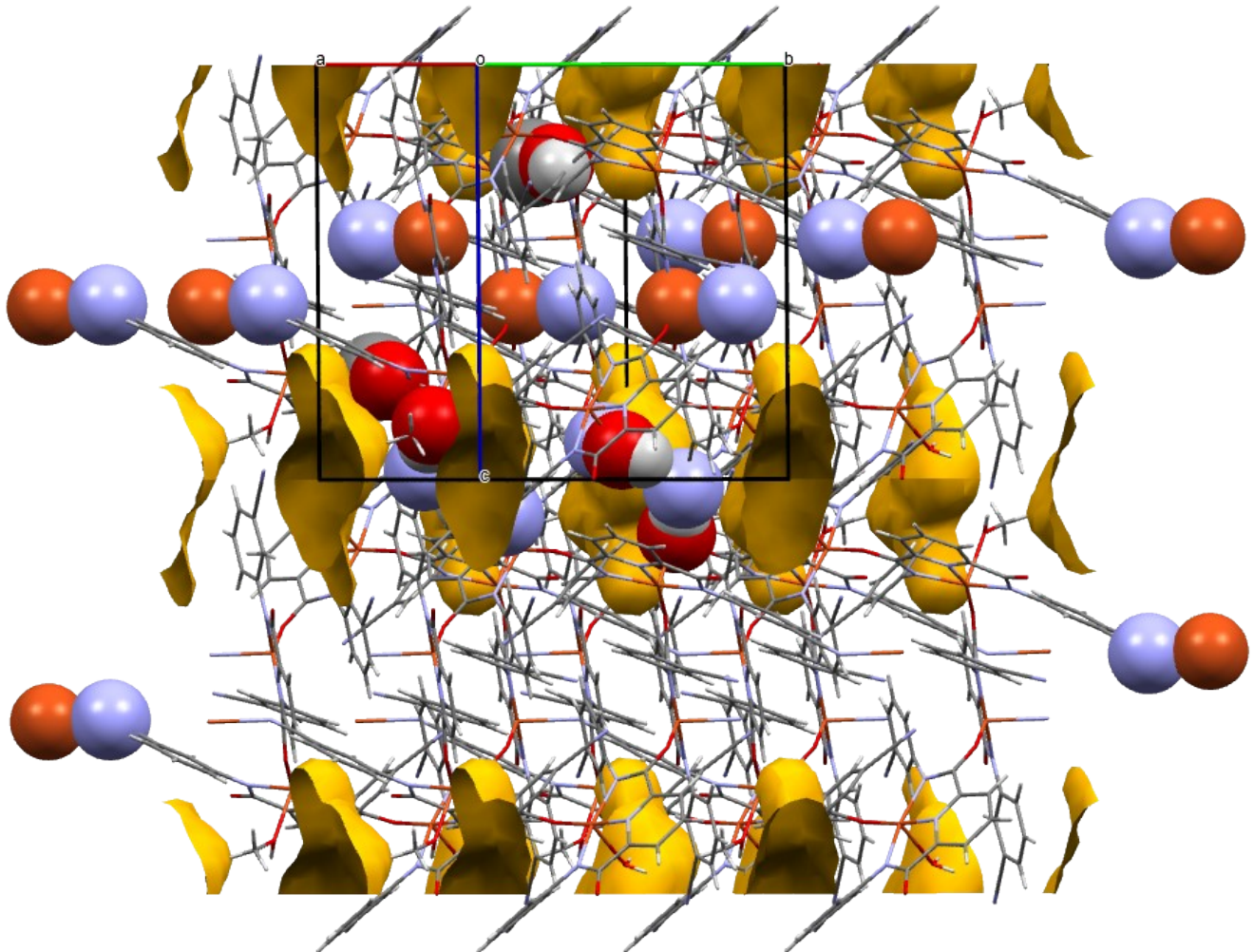


**S5.1**: The unit cell and packing of **Cu1** supermolecules in the crystal lattice. The intermolecular interactions have been shown as space-fill models and comprise of coordinating bonds that extend the hexamers as infinite polymers through the lattice. Additional C–H···O and H-bonding interactions further facilitate packing of the complex. The voids present in the crystal have also been shown and exist at the corners of the unit cell. The voids occupy 5.5% of the unit cell volume V = 2943.8 Å³.
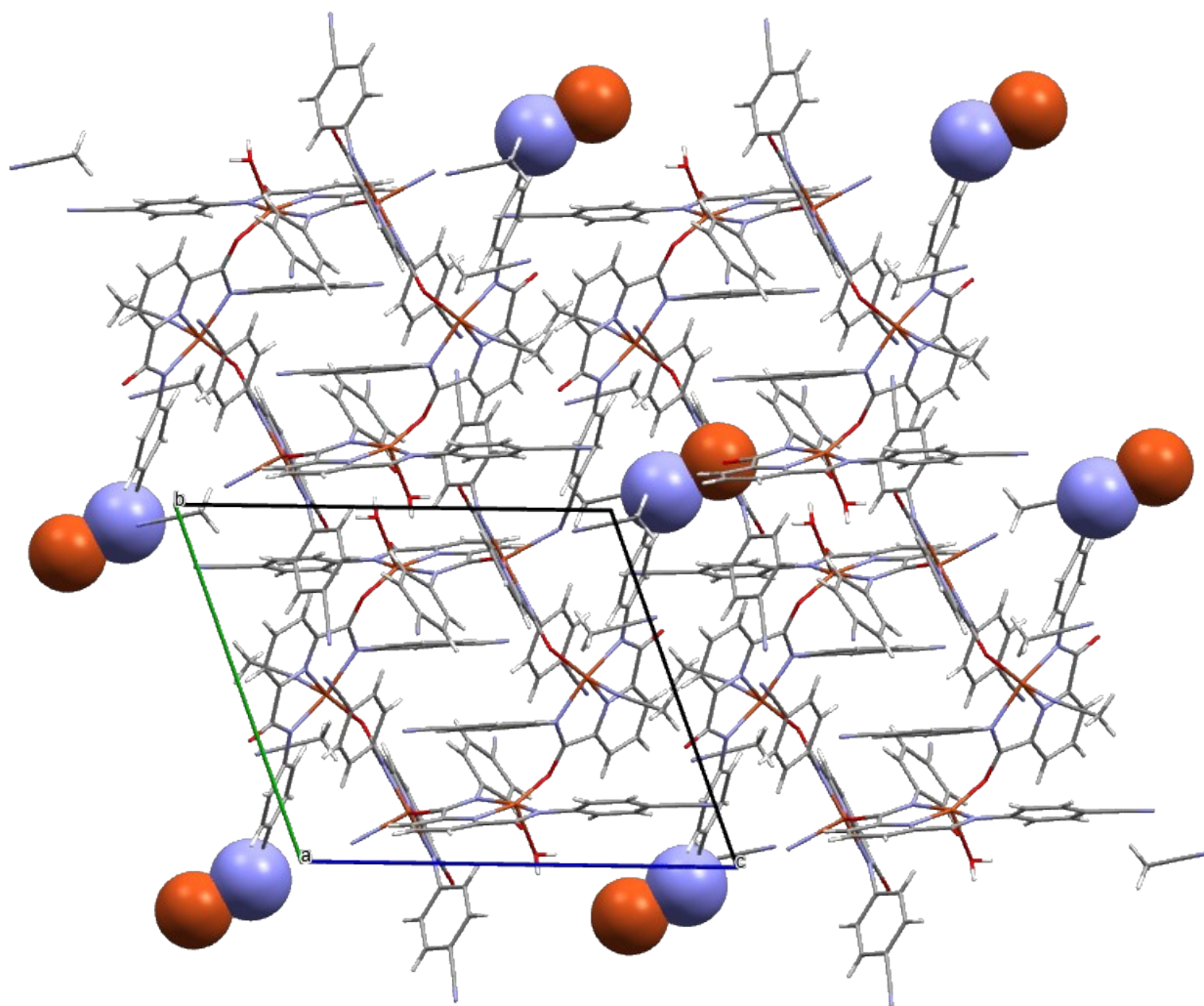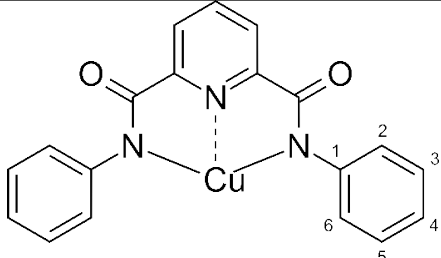
**S5.2**: The unit cell and packing of **Cu2** supermolecules in the crystal lattice. The intermolecular interactions have been shown as space-fill models and comprise of coordinating bonds that extend the hexamers as infinite polymers through the lattice along the crystallographic c-axis. Additional C–H···π and H-bonding interactions further facilitate packing of the complex. There are no voids in the crystal of **Cu2** as the 4-position nitrile packs more efficiently than the 3-position nitrile present on **Cu1**.
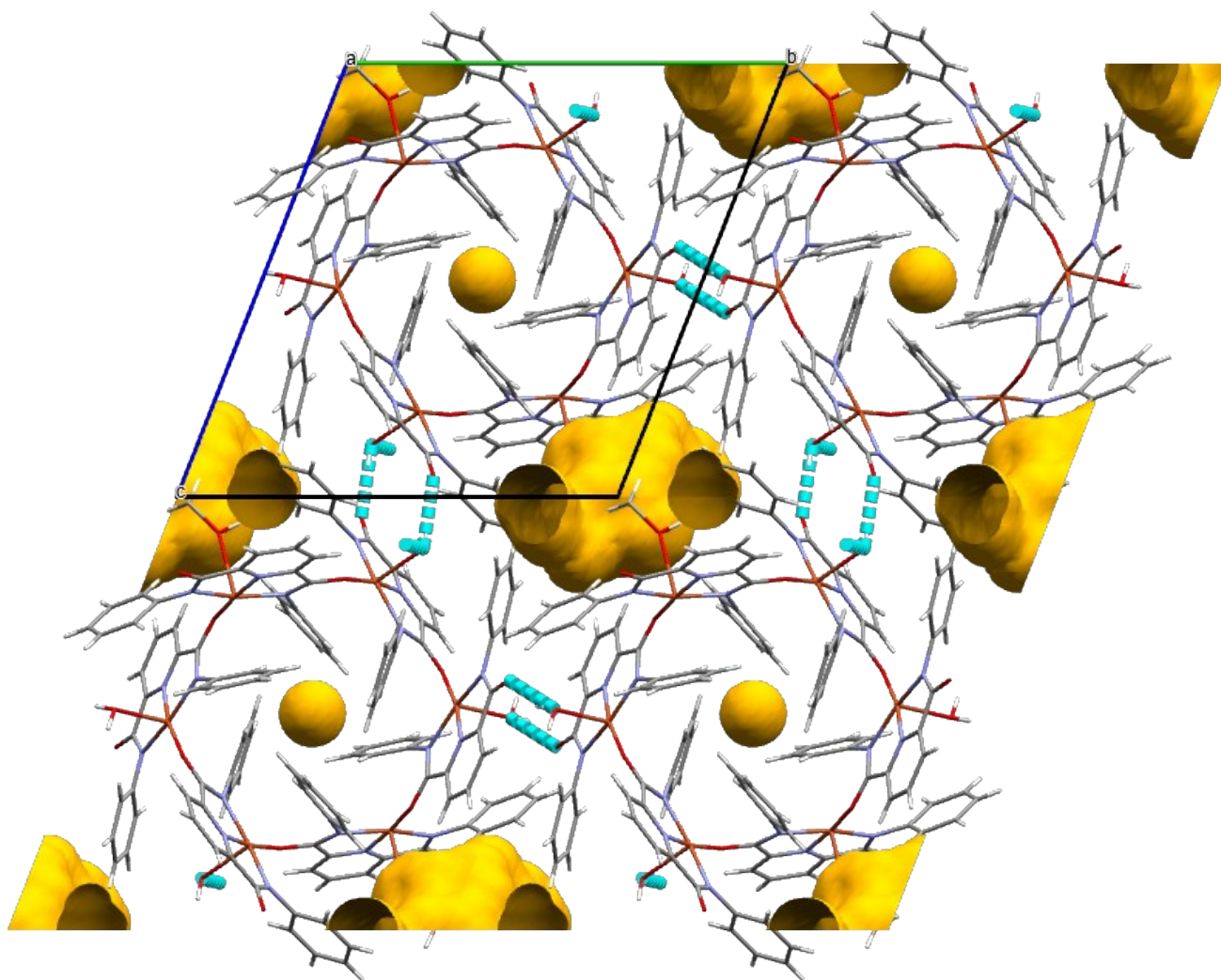
**S5.3**: The unit cell and packing of **Cu3** supermolecules in the crystal lattice. The intermolecular interactions comprise of H-bonding between axially bound aqua ligands and amide carbonyls of neighboring metallocycles. The voids present in the crystal have also been shown and exist as irregular cavities along the unit cell as well as a sphere at the center of the metallocycle. The voids occupy 6.7% of the unit cell volume V = 2793.0 Å$^3$.

# S6 CSD

Table S1: CSD results upon submission of the search query. The aryl substitution positions have been labelled on the query structure. Reference codes highlighted in green represent structures that possess H-bond donors on the chelate.

| CSD Analysis Copper NNN Amide Pincers | | | | |
|---|---|---|---|---|
| Search Query |  | | | |
| CSD Reference Code | Coordination Number | Charge | Aryl Substitution Pos. | Extended Structure |
| ANICIM | 4 | Neutral [Cu(III)] | 2,6 | Monomer |
| ANICOS | 4 | Neutral [Cu(III)] | 2,6 | Monomer |
| ANICUY | 4 | Anion | 2,6 | Monomer |
| ANIDAF | 4 | Anion | 2,6 | Monomer |
| ANIDEJ | 4 | Anion | 2,6 | Monomer |
| AWUNEN | 4 | Anion | 2,6 | Monomer |
| CATDAG | 4 | Anion | 2,6 | Monomer |
| CATDEK | 4 | Neutral [Cu(III)] | 2,6 | Monomer |
| DOWSAM | 5 | Anion | 2,6 | Monomer |
| DUVCAA | 5 | Anion | 2,6 | Monomer |
| DUVCEE | 4 | Anion | 2,6 | Monomer |
| EFAFID | 5 | Neutral | 2,6 | Monomer |
| EFAFOJ | 5 | Neutral | 2,6 | Monomer |
| EFAKAA | 4 | Anion | 2,6 | Monomer |
| HIHQEW | 5 | Neutral | 2,6 | Monomer |
| HIHVIF | 4 | Anion | 2,6 | Monomer |
| HIYWAQ | 4 | Anion | 2,6 | Monomer |
| HOCXIJ | 4 | Anion | 2,6 | Monomer |
| HOCXOP | 4 | Anion | 2,6 | Monomer |
| HUCFET | 5 | Neutral | 2 | Monomer |
| HUTMUH | 5 | Neutral | 2,6 | Monomer |
| HUTNUI | 4 | Neutral | 2,6 | Monomer |
| IBEXEU | 4 | Anion | 2,6 | Monomer |
| IBEXIY | 4 | Anion | 2,6 | Monomer |
| IBEXOE | 4 | Neutral | 2,6 | Monomer |
| IBEXUK | 4 | Neutral | 2,6 | Monomer |
| JOSQAJ | 5 | Neutral | 2 | Monomer |
| KAJLIT | 4 | Anion | 2,4,6 | Monomer |
| KAJLOZ | 5 | Neutral | 2,4,6 | Monomer |
| KAJLUF | 5 | Neutral | 2,4,6 | Monomer |
| KAJMAM | 4 | Neutral | 2,4,6 | Monomer |

| | | | | |
|---|---|---|---|---|
| MEQQEF | 5 | Neutral | 2 | Monomer |
| MIHJEU | 4 | Anion | 2,6 | Monomer |
| MIHJIY | 4 | Anion | 2,6 | Monomer |
| MIJFUI | 4 | Anion | 3 | Dimer |
| MIMDAQ | 5 | Neutral | 2 | Dimer |
| MIMDEU | 4 | Neutral/Anion | 2 | Dimer |
| MIMFIA | 4 | Anion | 2 | Dimer |
| MOWCUZ | 5 | Anion | 2,6 | Monomer |
| OPIHUT | 4 | Anion | 2,6 | Monomer |
| OSIDAW | 4 | Neutral | 2,6 | Monomer |
| QAWQOY | 5 | Anion | 2,6 | Monomer |
| QOCXIS | 4 | Anion | 2 | Dimer |
| QOFLAB | 4 | Anion | 2,6 | Monomer |
| QOFLIJ | 4 | Anion | 2,6 | Monomer |
| QOFLOP | 5 | Anion | 2,6 | Monomer |
| QOFLUV | 4 | Anion | None | Dimer |
| QOFMAC | 4 | Anion | 3 | Dimer |
| QOFMEG | 4 | Anion | 2,6 | Monomer |
| QOFMIK | 4 | Anion | 2,6 | Monomer |
| REKYOX | 4 | Anion | 2,6 | Monomer |
| REKYUD | 4 | Anion | 2,6 | Monomer |
| REVQEQ | 5 | Neutral | 2 | Monomer |
| SEQZAR | 4 | Neutral | 3 | Monomer |
| SEQZOF | 4 | Anion | 3 | Monomer |
| SEQZUL | 4 | Anion | 3 | Monomer |
| TEGVOT | 4 | Anion | 2,6 | Monomer |
| TEGVUZ | 4 | Anion | 2,6 | Monomer |
| TOZFEW | 5 | Anion | 2,6 | Monomer |
| UGAKOF | 4 | Anion | 2,4,6 | Dimer |
| UGALIA | 4 | Anion | 2,4,6 | Monomer |
| UGALOG | 4 | Neutral | 2,4,6 | Monomer |
| VOLPOD | 4 | Anion | 2 | Monomer |
| VOLPUJ | 4 | Neutral | 2 | Dimer |
| VULDEO | 4 | Anion | 2,6 | Monomer |
| VULDIS | 4 | Anion | 2,6 | Monomer |
| VULDOY | 4 | Anion | 2,6 | Monomer |
| VULDUE | 4 | Neutral [Cu(III)] | 2,6 | Monomer |
| VULFAM | 4 | Neutral [Cu(III)] | 2,6 | Monomer |
| VULFEQ | 4 | Neutral [Cu(III)] | 2,6 | Monomer |
| WOHSIV | 4 | Anion | None | Dimer |
| WOHSOB | 4 | Anion | None | Dimer |
| XIVGOY | 5 | Anion | 2 | Monomer |
| XIVGUE | 5 | Anion | 2 | Monomer |
| ZAZBUX | 5 | Neutral | 2 | Monomer |
| ZAZCAE | 4 | Neutral | 2 | Monomer |
| ZOFPOZ | 4 | Neutral | 2 | Monomer |

| ZOFPUF | 4 | Neutral | 2 | Monomer |
|---|---|---|---|---|
| **Cu1** | 5 | Neutral | 3 | Hexamer |
| **Cu2** | 5 | Neutral | 4 | Hexamer |
| **Cu3** | 5 | Neutral | None | Hexamer |

Table S2: Crystallographic data.

| Crystal Data | **Cu1** | **Cu2** | **Cu3** |
|---|---|---|---|
| Formula | $C_{128}H_{78}Cu_6N_{30}O_{16}$, 1.5[$CH_3OH$] | $C_{130}H_{76}Cu_6N_{32}O_{14}$, 4[$C_2H_3N$] | $C_{114}H_{86}Cu_6N_{18}O_{16}$, $C_2H_6O_2$, 5[$CH_3OH$] |
| Cell | Triclinic | Triclinic | Triclinic |
| Space Group | P-1 | P-1 | P-1 |
| Mr /g mol−1 | 2721.50 | 2855.68 | 2567.52 |
| a / Å | 12.8621(7) | 14.4764(11) | 10.8153(11) |
| b / Å | 14.6778(8) | 15.1477(11) | 17.0091(16) |
| c / Å | 17.1404(9) | 16.4380(10) | 17.4196(16) |
| α / ° | 76.085(2) | 106.667(3) | 106.568(5) |
| β / ° | 70.053(2) | 95.920(3) | 100.629(5) |
| γ / ° | 81.249(2) | 110.424(3) | 107.750(5) |
| Z | 1 | 1 | 1 |
| V / Å3 | 2943.8(3) | 3152.1(4) | 2793.0(5) |
| Voids / % | 5.5 | 0 | 11 |
| R1 / % | 3.6 | 4.82 | 6.8 |